JCB Article

Microtubules provide directional cues for polarized axonal transport through interaction with kinesin motor head

Takao Nakata and Nobutaka Hirokawa

Department of Cell Biology and Anatomy, Graduate School of Medicine, University of Tokyo, Tokyo, Japan 113-0033

Post-Golgi carriers of various newly synthesized axonal membrane proteins, which possess kinesin (KIF5)-driven highly processive motility, were transported from the TGN directly to axons. We found that KIF5 has a preference to the microtubules in the initial segment of axon. Low dose paclitaxel treatment caused missorting of KIF5, as well as axonal membrane proteins to the tips of dendrites. Microtubules in the initial segment of axons showed a remarkably high affinity to EB1–YFP, which was known to bind the tips of growing microtubules. These findings revealed unique features of the microtubule cytoskeletons in the initial segment, and suggested that they provide directional information for polarized axonal transport.

Introduction

Neurons are highly polarized cells with dendrites and a long axon. Intracellular transport of various kinds of membrane organelles and protein complexes are fundamental for neuronal morphogenesis, function, and survival. Recently, it has been revealed that a number of kinesin super family proteins (KIFs) play significant roles on these transports (Hirokawa, 1998). Axons in long tracts are as long as 1 m in humans, constituting more than 99% of the volume of the cells. In contrast, the diameter of an axon at a cell body of a mature neuron is often very small, and accordingly, axonally transported materials should be propelled from the cell body to the range only 0.25% of all the directions in order to enter the axon if we assume that the diameter of an axon is one-tenth of that of the cell body. Thus, it is natural to assume that there will be a molecular mechanism for the axonal vesicles to find a way to axons, but it was unknown even whether such selective polarized axonal transport exists within the cell body, and current models for polarized transport in neurons underestimate it (Jareb and Banker, 1998; Burack et al., 2000). Previously, we have shown that the transport of newly synthesized proteins from Golgi complexes to the cell surface is mediated by tubulovesicular organelles in axons, which was subsequently confirmed in both neurons (Nakata et al., 1998; Zakharenko and Popov, 1998; Ahmari et al., 2000; Kaether et al., 2000) and nonneuronal cells (Hirschberg et al., 1998; Toomre et al., 1999). However, it was difficult to analyze the transport within the cell body at high spatial and temporal resolution because of high background due to the ER retention or the overexpression of the protein. Thus, the behavior of post-Golgi axonal and dendrite carriers has not been visualized within the cell body in detail, which is critical for building models for polarized transport in neurons. In this paper, we overcame these difficulties by the improvement of marker proteins and critical angle fluorescence microscopy (CAFM), which enables us to observe inside cells deeper than with the strict total internal reflection (TIR) microscopy and to eliminate most of the background signals. We demonstrated the evidences that axonal post-Golgi carriers in the cell body know the direction of the axon and microtubules (MTs) provide the directional cues for the polarized axonal transport.

Results

Polarized axonal transport in neurons

Previously, axonally transported vesicles were considered to be transported nonselectively into both dendrites and axons because vesicles, which carry axonal membrane protein–GFP

Address correspondence to Nobutaka Hirokawa, Dept. of Cell Biology and Anatomy, Graduate School of Medicine, University of Tokyo, 7-3-1, Hongo, Tokyo, Japan 113-0033. Tel.: 81-3-5841-3326. Fax: 81-3-5802-8646. email: hirokawa@m.u-tokyo.ac.jp

Key words: critical angle fluorescent microscopy; paclitaxel; polarized sorting; EB1; neurons

Abbreviations used in this paper: CAFM, critical angle fluorescent microscopy; CLSM, confocal laser scan microscopy; IS, initial segment of axon; MAP, MT-associated protein; MT, microtubule; TIR, total internal reflection; VSV-G, vesicular stomatitus virus G-protein.

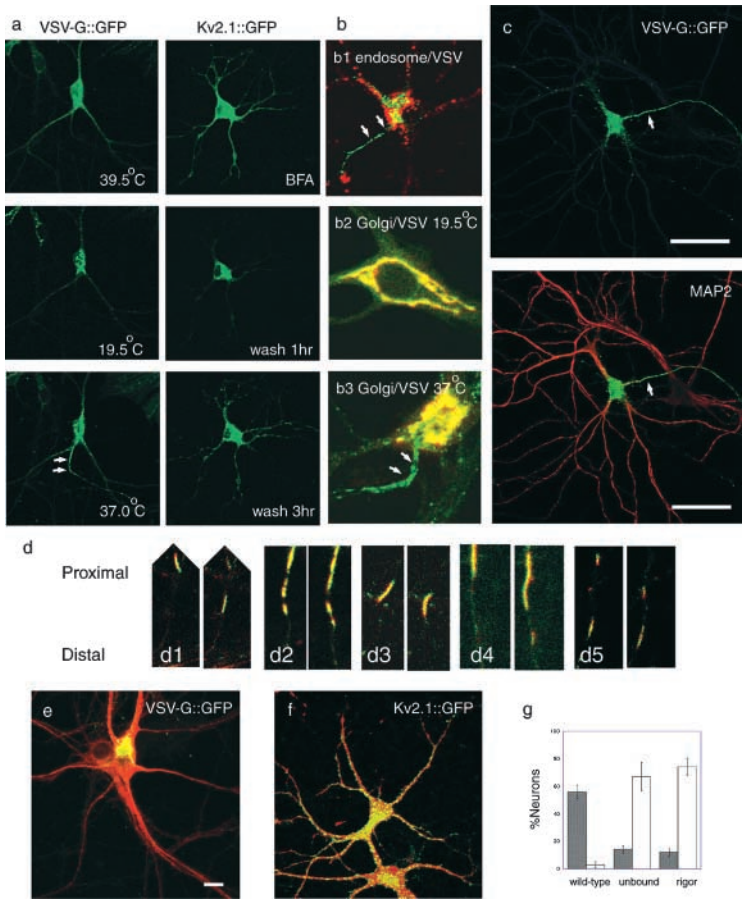

Figure 1. **Post-Golgi transport of axonal and dendrite carriers in hippocampal neurons visualized by CLSM.** (a) Sorting of membrane protein–GFP fusion proteins under specific cell manipulation. VSVtsO45-G::GFP localizes in the ER at 39.5°C and moves to the TGN after a 30-min incubation at 19.5°C. Its post-Golgi transport starts when the temperature is shifted to 37°C. Note that VSV-G::GFP carriers are predominantly transported to one neurite (arrows) among the others. Kv2.1::GFP distributes diffusely in the somatodendritic area when expressed overnight in the presence of 1 μM brefeldin A. Kv2.1::GFP accumulates at the Golgi region 1 h after the brefeldin A washout, and starts post-Golgi transport. Note that Kv2.1::GFP was transported to all the dendrites 3 h after wash. (b) Characterization of VSV-G::G(Y)FP probes in neurons. (b1) Neurons were infected with Ad(VSVtsO45-G::GFP) and incubated overnight at 39.5°C, for 30 min at 19.5°C, and for 1 h at 37°C in the presence of 1 mg/ml Texas-red dextran (MW3000). Note that post-Golgi VSV-G carriers in the axon (arrows, green) are not labeled with the endocytotic marker (red). (b2 and b3) Double-label of hippocampal neuron with VSV-G::YFP and Golgi–CFP. At 19.5°C (b2), VSV-G::YFP (b2, green) was colocalized with the Golgi complex marker (b2, red) in the cell body. When the temperature is shifted to 37°C (b3), VSV-G::YFP moves from the Golgi complex area (yellow area at the upper right of b3, due to the overlap of VSV-G::YFP [green] and Golgi–CFP [red]) to the axon (b3, arrows). (c) VSV-G::GFP was dominantly transported from the TGN to the axon (arrow). Neurons were infected with Ad(VSVtsO45-G::GFP) and incubated overnight at 39.5°C, for 30 min at 19.5°C, and for 1 h at 37°C to visualize post-Golgi membrane transport (green). After fixation, the dendrites were stained with the anti-MAP2 antibody (red). Bar, 50 μm. Videos 1 and 2 are available at http://www.jcb.org/cgi/content/full/jcb.200302175/DC1. (d) Post-Golgi axonal carriers of VSV-G::GFP transport various membrane proteins. Axonally transported tubulovesicular organelles were simultaneously double-labeled with CFP- and YFP-tagged proteins, and time-lapse data were collected by sequential activation with 442 and 488 nm lasers by CLSM. (d1) VSV-G::CFP::CFP (red) and GAP-43::YFP (green). (d2) VSV-G::CFP::CFP (red) and β-APP::YFP (green). (d3) VSV-G::YFP (green) and Vamp2::CFP (red). (d4) Vamp2::CFP (red) and GAP-43::YFP (green). (d5) Vamp2::CFP (red) and β-APP::YFP (green). In each set, interval between the right and left panel is 10 s. Slight gaps between the CFP and YFP images along the longitudinal axis of vesicles are due to the time lag (~0.7 s) between the sequential data acquisition. (e and f) Dominant negative kinesin (S205A,H206A; stained with the H2 antibody; red) inhibits polarized axonal transport of VSV-G::GFP (e, green), whereas it does not inhibit significantly dendrite transport of Kv2.1::GFP (f, green). Bars, 10 μm. (g) Inhibition of polarized axonal transport by dominant negative kinesins. Black bars indicate percentage of neurons with polarized VSV-G::GFP transport, and white bars indicate percentage of neurons exhibiting accumulation of VSV-G::GFP at TGN. Data were collected from four independent cultures.

fusion proteins often accumulated in both dendrites and axons (Jareb and Banker, 1998). This may be due to a small amount of missorted proteins, which finally accumulated at the time of observation in the somatodendritic area with a limited volume because they cannot be exocytosed to dendrite membranes. To eliminate these effects, we used temperature-sensitive vesicular stomatitis virus G-protein (VSV-G tsO45; Hirschberg et al., 1998; Toomre et al., 1999). We expressed VSV-GtsO45::GFP at 39.5°C overnight, allowed it to accumulate in the Golgi apparatus by decreasing the temperature to 19.5°C, and monitored the post-Golgi transport at 37°C (Fig. 1 a; Videos 1 and 2, available at http://www.jcb.org/cgi/content/full/jcb.200302175/DC1). Double label with Golgi–CFP (CLONTECH Laboratories, Inc.) and VSV-G::YFP revealed that VSV-G::YFP colocalized with the Golgi complex–marker at 19.5°C (Fig. 1, b2), and post-Golgi VSV-G::YFP carriers moved predominantly to one neurite from the Golgi region after temperature shift to 37°C (Fig. 1, b3, arrows). This temperature shift protocol was used for VSV-G throughout the experiment. These carriers were not labeled with endocytotic marker Texas red dextran (Fig. 1, b1, arrows). This result, together with previous papers, indicates that these carriers are not derived from endosomes (Nakata et al., 1998; Ahmari et al., 2000). Although VSV-G itself is sorted to dendrites (Dotti and Simons, 1990), we found that VSV-G tsO45 was sorted to axons in hippocampal neurons when tagged with GFP in its COOH terminus as shown by staining of dendrites with anti–MT-associated protein (MAP) 2 antibody (Fig. 1 c). Thus, we used VSV-G::GFP as an axonal transport marker. Simultaneous expression of CFP and YFP fusion proteins revealed that VSV-G::GFP was transported by the tubulovesicular organelles, which transport a number of newly synthesized axonal membrane proteins such as β-APP, GAP-43, and vamp-2 (Fig. 1 d), indicating that VSV-G tsO45::GFP labels major post-Golgi carriers for various axonal membrane proteins (Nakata et al., 1998). Number of vesicles entered axons is 3.8 times more than those to any dendrites in average. We judged the transport is polarized if it is more than twice as much as those to any dendrites. We found that

VSV-G::GFP was transported in a polarized manner in ~60% of neurons (Fig. 1 g and Fig. 5 j), indicating that there is a mechanism for polarized vectorial axonal transport.

Next, we compared the polarized axonal transport with dendrite transport within the cell body. Because the construct with longer spacers is reported to reduce the effect of GFP tagging on VSV-G sorting in MDCK cells (Keller et al., 2001), we tried the same construct to test whether it could be a marker for dendrite transport. However, its effect was insufficient in the neurons, and a considerable amount of the protein was still sorted to axons (unpublished data). We used Kv2.1::YFP, a potassium channel that is sorted to somatodendritic plasma membrane (Lim et al., 2000), in order to visualize individual post-Golgi dendrite carriers. Among the number of channels and receptors we tried, most of which showed considerable amount of ER retention, which obscured the observation of the post-Golgi dendrite transport, Kv2.1::YFP was accumulated in the Golgi region by brefeldin A washout treatment (Fig. 1 a), which enabled us to follow the subsequent post-Golgi transport. Brefeldin A washout procedure did not affect on sorting as well as the time course of distribution of Kv2.1::YFP within dendrites and used in Fig. 1 a and Fig. 2 (a–e). Simultaneous expression of VSV-G::CFP::CFP and Kv2.1::YFP showed each markers are properly targeted to axonal and dendrite carriers while they are colocalized in the Golgi region (Fig. 2 f). We used CAFM (see Materials and methods), which enabled us to visualize small dim dendrite vesicles that our confocal laser scan microscopy (CLSM) system could not visualize. Our CAFM image of biased axonal transport of VSV-G was fully consistent with the CLSM image. Intense staining in the center of the cell body in Fig. 2 (a and b) are the basal surface of the Golgi region demonstrating the depth of CAFM image from the coverslip. We found that VSV-G carriers were tubular and vesicular in shape, highly motile with long processivity, and preferentially transported to axons (Fig. 2 a; Video 3, available at http://www.jcb.org/cgi/content/full/jcb.200302175/DC1), whereas Kv2.1 carriers were vesicular in shape, less motile with short processivity, and evenly distributed within the cell body (Fig. 2 b; Video 4, available at http://www.jcb.org/cgi/content/full/jcb.200302175/DC1). Comparison of percentage of the carriers with >1 μm displacements in 10 s showed that VSV-G carriers have much higher motile activity than Kv2.1 carriers (Fig. 2 c), which results in the smaller number of VSV-G carriers remaining in the cell body (Fig. 2 d). These differences are not due to the time-lapse imaging at a 5-s interval, as the time-lapse video with a 0.5-s interval (Video 5, available at http://www.jcb.org/cgi/content/full/jcb.200302175/DC1) showed the same tendency of Kv2.1 carrier movements. Next, we compared the run-length of each 100 individual carriers before they stop or change the direction of movements (Fig. 2 e). We found ~50% of VSV-G carriers show >5 μm processive movements, whereas >50% of Kv2.1 carriers show <1 μm processivity. Given the average run-length of single kinesin motor proteins ~0.6 μm (Vale et al., 1996), the data indicate that multiple active motors are associated with a single VSV-G carrier. This motile property of VSV-G carriers will be suitable for the polarized axonal transport because once the carriers choose the axonal MTs, they will continue to translocate along them until they get out of the cell body.

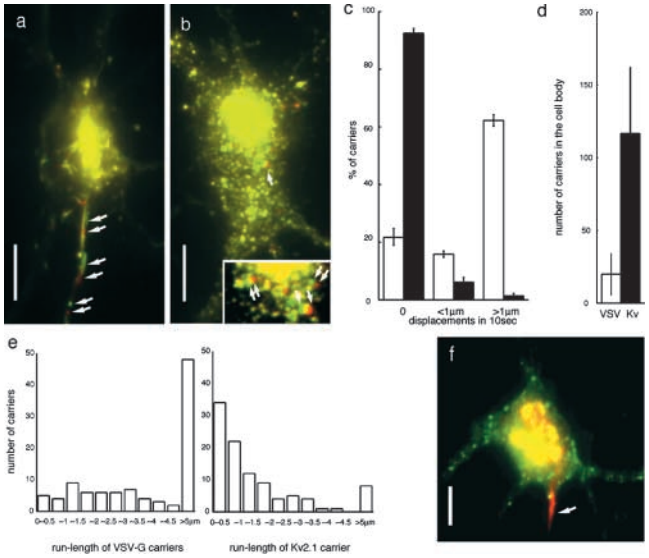

Figure 2. **Analysis of axonal and dendrite carrier movement by CAFM.** CAFM images of the post-Golgi complex carriers to the axon (a: VSV-G::GFP) and to the dendrites (b: Kv2.1::GFP). Two images at 10-s intervals were merged into one image to show the displacements of individual carriers for 10 s (red images are obtained 10 s later than the green images). Axonal tubulovesicular organelles showed high motility and dominantly transported to the axon (arrows in a indicate three moving carriers). In contrast, post-Golgi carriers for Kv2.1 were vesicular in shape and do not show directional preference in motility (inset in b shows a high magnification of the area indicated by an arrow. Three moving carriers are indicated by arrows in the inset. Note carriers with displacements less than their diameter show overlapping yellow region of two merged images). Corresponding videos are available as Videos 3–5. (c–e) Quantitative analysis of the dynamics of axonal versus dendrite carriers. (c) Percentage of the carriers which shows 0 μm, <1 μm, >1 μm displacements in 10 s in the cell body. Black bar, Kv2.1 carriers; white bar, VSV-G carriers. Data were obtained from three independent cultures. 200 carriers were counted in each culture. (d) Number of the post-Golgi carriers remaining within the cell body. Carriers were counted at 1 h after the start of the post-Golgi transport. Black bar, Kv2.1 carriers; white bar, VSV-G carriers. (e) Histogram of the run-length of individual 100 post-Golgi carriers of Kv2.1 and VSV-G. Carriers, which showed no displacement, were omitted from the histogram. Carriers, which move into neurites and get out of the observing field, were included in the group of >5 μm run-length. (f) Simultaneous double labeling with Kv2.1::YFP (green) and VSV-G::CFP::CFP (red). Note that they colocalize in the Golgi complex area. Kv2.1 carriers distributed in the somatodendritic area, but VSV-G carriers move to the IS (arrow). Bars, 10 μm.

KIF5 has been shown to transport VSV-G::GFP (Kreitzer et al., 2000), β-APP (Kaether et al., 2000; Kamal et al., 2000), and GAP-43 (Ferreira et al., 1992). We confirmed it by the dominant negative approach. When the full length of KIF5 with mutations at both S205A and H206A, which dissociates kinesin from MTs, is overexpressed in hippocampal neurons, transport of VSV-G::GFP from the TGN was inhibited (Fig. 1, e and g). Rigor-KIF5 (T93N) also inhibited the transport, whereas overexpression of wild-type kinesin did not (Fig. 1 g). In contrast, transport of Kv2.1::YFP was not significantly affected by the dominant negative KIF5

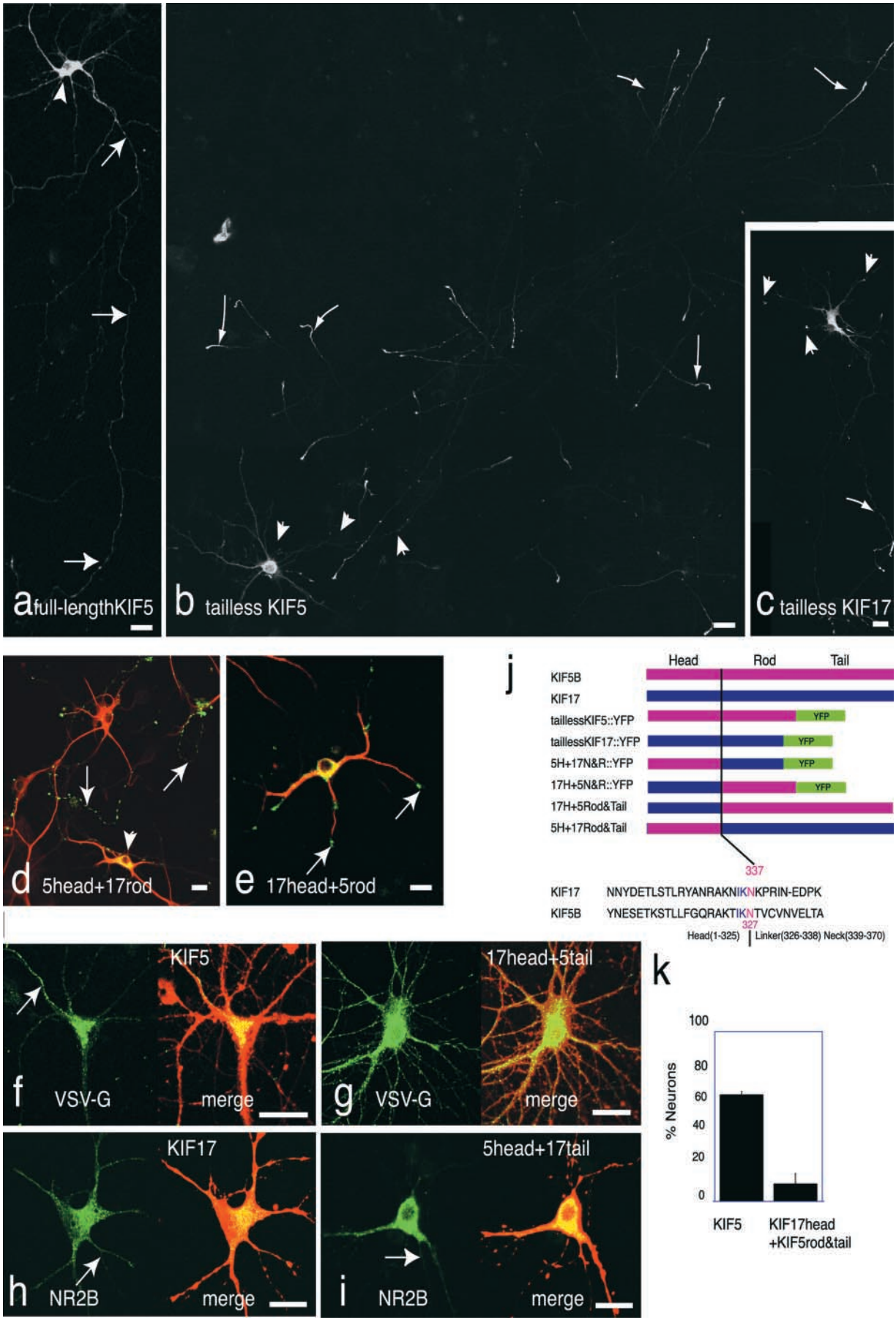
a full-length KIF5
b tailless KIF5
c tailless KIF17
d 5head+17rod
e 17head+5rod
j
Head
Rod
Tail
KIF5B
KIF17
taillessKIF5::YFP
taillessKIF17::YFP
5H+17N&R::YFP
17H+5N&R::YFP
17H+5Rod&Tail
5H+17Rod&Tail
YFP
337
KIF17 NNYDETLSTLRYANRAKNIKNKPRIN-EDPK
KIF5B YNESETKSTLLFGQRAKTIKNTVCVNVELTA
327
Head(1-325) Linker(326-338) Neck(339-370)
f KIF5
VSV-G
merge
g 17head+5tail
VSV-G
merge
k
100
80
60
40
20
0
% Neurons
KIF5
KIF17head
+KIF5rod&tail
h KIF17
NR2B
merge
i 5head+17tail
NR2B
merge

construct (Fig. 1 f). These results, together with previous reports (Ferreira et al., 1992; Kaether et al., 2000; Kamal et al., 2000; Kreitzer et al., 2000), indicate that conventional kinesin is the motor for the axonal transport of tubulovesicular organelles containing VSV-G::GFP.

Sorting of kinesin in neurons

Because our observation suggested that VSV-G carriers are driven by a number of active KIF5 motors, we tested whether KIF5 itself has a property to find its preferential way to the axons. When the full-length KIF5::GFP fusion protein was expressed in hippocampal neurons, a considerable amount of KIF5::GFP was localized in the cell body and dendrites (Fig. 3 a; see Fig. S1 for double label image with axonal marker, available at http://www.jcb.org/cgi/content/full/jcb.200302175/DC1), consistent with the immunocytochemical localization of kinesin (Kanai et al., 2000). Simple localization of kinesin does not reveal the actual site of action of kinesin because recent studies showed that most of the kinesin remains inhibited from binding to MTs by the association of its motor domain with its tail domain (Coy et al., 1999; Hackney and Stock, 2000), and unbound kinesin will be subject to simple diffusion. We eliminated the effect of tail inhibition as well as cargo binding, by deleting the tail and COOH-terminal region of the rod domain (Seiler et al., 2000). The localization of tailless motor proteins can be attributed simply to their motor activity. In fact, these motors are shown to accumulate at the tips of processes (Seiler et al., 2000). Although MT polarity is mixed in the proximal area of dendrites, it is plus end–directed in both the axons and distal parts of dendrites (Baas et al., 1988). If motor proteins do not discriminate MTs, they will run on both axonal and dendrite MTs toward the plus ends, and should accumulate at both axon and dendrite tips. When the tailless KIF5B::GFP fusion protein was expressed, the protein accumulated at the tips of axons, with a marked decrease in its level in dendrites (71 of 84 transfected neurons; Fig. 3 b; see Fig. S1 b for double label image with CFP). Total amount of GFP motor in axonal tips shown in Fig. 3 b was 3.14-fold higher that in the whole dendrites. This was confirmed in all the members of the KIF5 subfamily (KIF5A-C) in mouse. Various KIFs proteins are involved in axonal versus dendrite transport (Miki et al., 2001). We found that KIF17, an MT-plus end–directed motor transporting glutamate receptor NR2B in dendrites (Setou et al., 2000), accumulated at the tips of both dendrites and axons when their tail domains were deleted (41 of 47 tailless KIF17 transfected neurons; Fig. 3 c; see Fig. S1 c for double label image with dendrite marker). The accumulated KIFs were extracted by mild saponin extraction in the presence of paclitaxel without ATP (unpublished data), indicating that their accumulation is not due to strong binding to MTs in the distal (Nakata and Hirokawa, 1995). Chimera proteins with the KIF5 head and KIF17 neck and rod accumulated at the tips of axons (Fig. 3, d and j), whereas chimera proteins with KIF17 head and KIF5 neck and rod accumulated in both axons and dendrites (Fig. 3, e and j), indicating that the motor domain is a key to determine the KIF5 preference to axons. Motility of these chimera proteins was verified by in vitro motility assay (Fig. S2, available at http://www.jcb.org/cgi/content/full/jcb.200302175/DC1).

Next, we overexpressed chimera protein of the KIF17 head and KIF5 neck to tail domain in hippocampal neurons, and examined its effect on polarized axonal transport. In neurons, which overexpress full-length KIF5, polarized axonal transport was maintained (Fig. 3 f). Video 6 shows the VSV-G::GFP transport in the neuron presented in Fig. 3 f (Video 6, available at http://www.jcb.org/cgi/content/full/jcb.200302175/DC1). In contrast, when KIF17-KIF5 chimera protein was expressed, axonal carriers were transported in both axons and dendrites (Fig. 3 g; Video 7, available at http://www.jcb.org/cgi/content/full/jcb.200302175/DC1). The results suggest that the preferential axonal transport is attributed to the KIF5 motor domain. In contrast, tailless motor experiment indicates that motor domain preference does not explain the exclusion of dendrite carriers from axons because both tailless KIF5 and KIF17 were accumulated at the tips of axons. Indeed, NR2B::YFP was not missorted to axons when coexpressed with KIF5 head and KIF17 rod and tail construct (Fig. 3, h and i). Although KIF5 head has preference in axons and KIF17 head also can enter the axons, if there is a mechanism such as their cargo dissociates

Figure 3. **Tailless motors were destined for different regions of neurons.** Data were obtained by CLSM. (a) Full-length KIF5B::GFP was transfected into hippocampal neurons. It was distributed throughout the cell body, dendrites, and the axon (arrows). The cell body and dendrites were brightly stained, just because of their thickness compared with the axon. (b) Tailless KIF5B::YFP were transfected into hippocampal neurons. Tailless KIF5B::YFP accumulated at the tips of axonal branches (arrows) but not dendrite tips. Cell body and proximal axon are indicated by arrowheads. (c) Tailless KIF17::YFP accumulated at the tips of dendrites (arrowheads) and axons (arrow). (d and e) Experiments on exchange of head domains revealed that head domains determine the destination of the tailless motors. MAP2 antibody is used as dendrite marker. (d) The KIF5B head and the KIF17 neck and rod constructs were destined for axons (green, arrows). The arrowhead indicates the cell body of transfected neuron. (e) The KIF17 head and the KIF5B neck and rod constructs were destined for the tips of dendrites (green). (f and g) Head exchange affects on polarized axonal transport. (f) Polarized axonal transport of VSV-G::GFP (green) was analyzed in the neurons that overexpress full-length KIF5B (red). VSV-G::GFP was preferentially sorted to the axon (arrow). (g) Preferential sorting of VSV-G::GFP (green, arrows) to the axon was inhibited in the neurons, which overexpress full-length KIF5 whose motor domain was replaced with KIF17 (red; see corresponding Videos 6 and 7). Fixation and immunocytochemistry to detect motor proteins was performed after live-cell imaging of VSV-G::GFP transport. (h and i) Head exchange does not affect on polarized dendrite sorting. NR2B::YFP distribution (green) was examined in the neurons, which overexpress authentic KIF17 (h, red) and full-length KIF17 whose motor domain was replaced with KIF5 (i, red). NR2B (green) was not sorted into axons in both cases. Arrows indicated the most likely candidates for axons. Bars, 10 μm. (j) Schematic diagram of the constructs. Head was exchanged at the border of head and neck-linker region of KIF5, and the corresponding region of KIF17 by the alignment. The colored amino acid sequences in the exchanged area were highly conserved. (k) Inhibition of polarized axonal transport by the head-exchanged KIF5. Bars indicate percentage of neurons with polarized β-APP::YFP transport. Data were collected from three independent cultures.

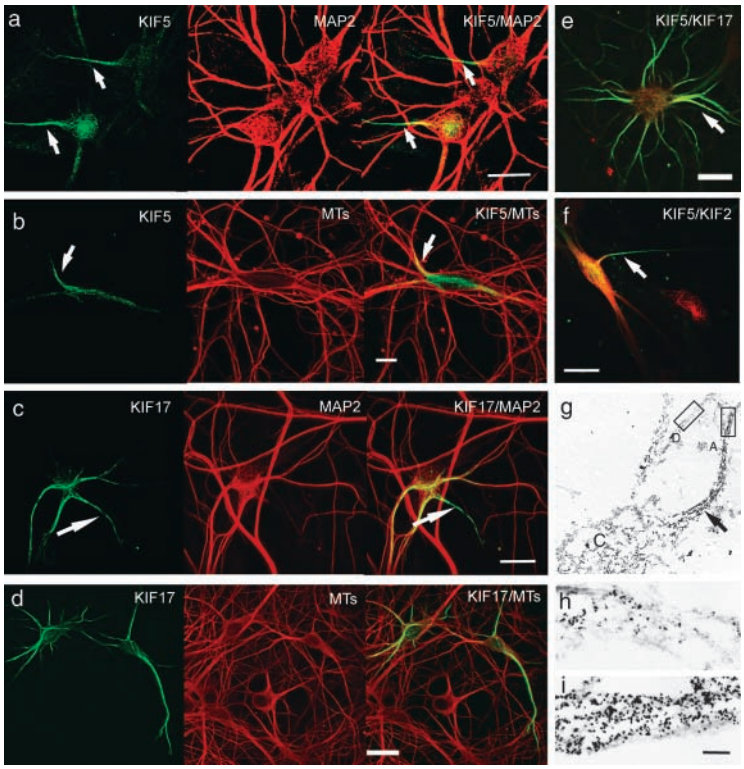

Figure 4. **KIF5 is preferentially recruited to the MTs in the IS.** After brief expression of rigor mutants of motor proteins, cells were permeabilized, fixed, and stained with antibodies. CLSM images of the strongly bound motors were obtained by serial Z-sectioning with a small confocal aperture to avoid the effect of the thickness of the cells. Data are presented as a maximal Z-projection image. Arrows indicate the IS. (a and b) Neurons expressing tailless KIF5B G234A::YFP (green) were stained with anti-MAP2 antibody (a, red) or with anti–β-tubulin antibody (b, red). Center of the cell body and the IS were intensely labeled by rigor-KIF5. (c and d) Neurons expressing tailless KIF17 G243A::YFP (green) were stained with anti-MAP2 antibody (c, red) and with anti–β-tubulin antibody (d, red). Dendrites as well as the IS (c, arrow) were intensely labeled with rigor-KIF17. (e) Simultaneous double-labeling with rigor-KIF5 (red) and tailless rigor-KIF17::YFP (green). KIF5 was stained with antikinesin antibody H2. Although the IS was intensely labeled by the both motors (arrow), KIF5 preferentially labels the center of the cell body, whereas KIF17 labels dendrites as well as axons. (f) Simultaneous double-labeling with rigor-KIF5 (green) and rigor-KIF2 (red). Although the labeling pattern in the cell body was similar in both KIFs, KIF5 preferentially labels the IS (arrow), whereas rigor-KIF2 does not. Bars, 10 μm. (g–i) Immunoelectron microscopy of rigor-KIF5 in hippocampal neurons. Rigor-KIF5 was labeled with 5-nm colloidal gold followed by silver enhancement. (g) Intense labeling of the IS is observable even at this low magnification (arrow). C indicates the cell body. (h) Higher magnification of the dendrite area in g (box D). (i) Higher magnification of axon area in g (box A). Note that extensive labeling of axons compared with dendrites. Bar, 500 nm.

from the motor when they entered into axons, the cargoes will be excluded from the axon.

Next, we addressed the question whether KIF5 is activated preferentially between TGN and axons. To test it, motor proteins that can be recruited to MTs but cannot translocate along nor dissociate from MTs are suitable because such mutant motor proteins will show the site of initial recruitment of the motor proteins by their localization. We know of three such point mutations of kinesin (rigor kinesins) that are well characterized (Nakata and Hirokawa, 1995; Rice et al., 1999). We found that all the mutations (T92N, G234A, and E236A) show the same results in the case of KIF5B. KIF5 G234A mutant and corresponding KIF17 G243A mutant were localized on MTs in transfected cells (Fig. S3, available at http://www.jcb.org/cgi/content/full/jcb.200302175/DC1). We expressed rigor-motor proteins fused with YFP in hippocampal neurons, permeabilized them in order to detect only MT-bound fractions. CLSM enabled us to compare the rigor-motor binding eliminating the effect of the difference in the thickness of axons and somatodendrites. We found that rigor-KIF5 with G234A mutation distributed most intensely on MTs from the center of the cell body to the initial segment of axon (IS), which is confirmed by MAP2 staining (Fig. 4 a; fluorescence ratios of rigor-KIF5::GFP axon to dendrites and dendrites to cell body were 217 ± 81.1% and 63.0 ± 20.8%, respectively [$n = 25$]). Double labeling with tubulin demonstrated relatively low density association of rigor-KIF5 with MTs in dendrites and high density association in the center of the cell body and the IS (Fig. 4 b; fluorescence ratios of rigor-KIF5::GFP to tubulin staining was 1.2 ± 0.4 [$n = 14$] in axons, and 0.5 ± 0.2 [$n = 22$] in dendrites). In contrast, rigor-KIF17 with corresponding G243 mutation distributed on MTs in both dendrites and the IS (Fig. 4 c). Double labeling with tubulin demonstrated high density association of the rigor-KIF17 with MTs in dendrites and the IS (Fig. 4 d). In the cell body, the rigor-KIF17 binds strongly to some MTs, but they show lower affinity with MTs in other areas of the cell body (fluorescence ratio of rigor-KIF17::YFP in axon to dendrites and dendrites to cell body were 109 ± 28.0% and 402 ± 281%, respectively [$n = 25$]). Simultaneous expression of rigor-KIF5 and rigor-KIF17 indicates that the preference of these two types is clearly different within the same neurons (Fig. 4 e). This distribution of rigor-KIF5 and -KIF17 is consistent with the destinations of tailless motors. Although motor domains of KIF5 and KIF17 had a property to bind to MTs in the IS, this is not always the case because rigor-KIF2 did not localize on MTs in the IS, as shown by the simultaneous expression of rigor-KIF2 and rigor-KIF5 in hippocampal neurons (Fig. 4 f). We further examined the axon preference of the rigor-KIF5 by using immunoelectron microscopy. Fig. 4 (g–i) shows biased binding of rigor-KIF5 to the IS (Fig. 4 g, arrow). These results suggest that KIF5 motor domain, as default, has a preference to the MTs in the IS and tailless KIF5 is preferentially sorted to axons.

Effects of low dose paclitaxel treatment

If the directional cue for the polarized axonal transport could be specifically blocked, we should expect that axonal

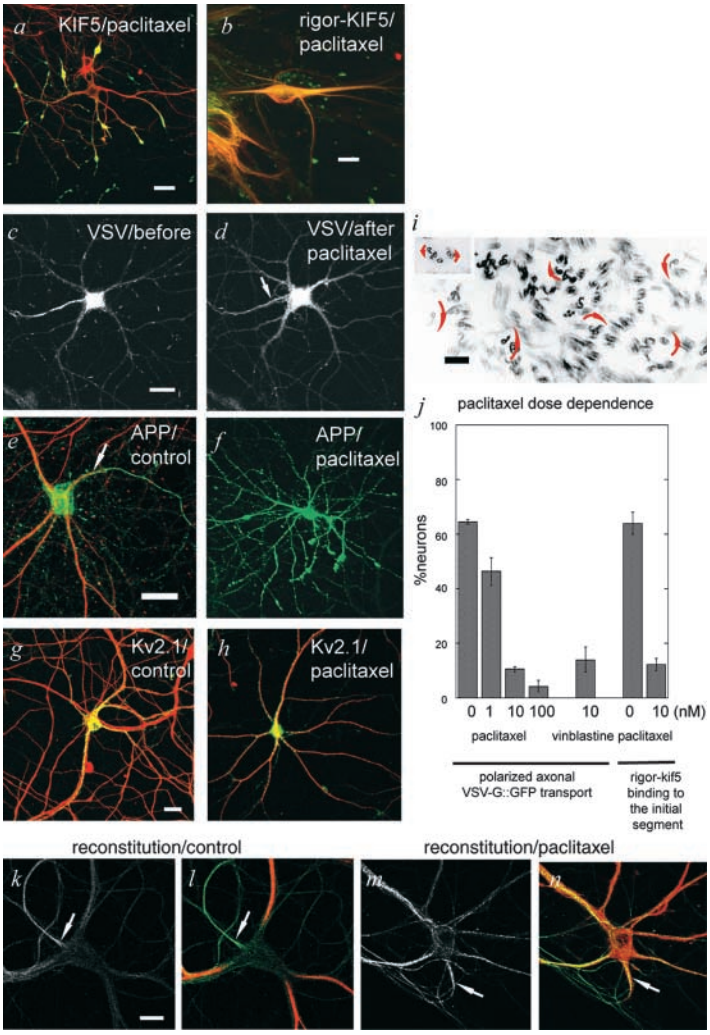

Figure 5. **Paclitaxel at a low dose reverts the polarized sorting of axonal motor proteins as well as membrane proteins.** Data were obtained by CLSM with small pinhole and maximal Z-projection (b, k, l, m, and n) and with pinhole fully open (a, c, d, e, f, g, and h). Arrows indicate axons. MAP2 (red) was stained in a, b, e, l, and m. (a) Tailless KIF5::YFP (green) was sorted to dendrite tips in the presence of 10 nM paclitaxel. (b) Rigor-KIF5::YFP (green) failed to accumulate in the IS in the presence of 10 nM paclitaxel. (c and d) VSV-G::GFP was initially observed 1 h after the temperature shift to 30°C from 19.5°C without paclitaxel (c), and 10 nM paclitaxel (d) was added to the medium. Axonal transport from the IS was unchanged. However, as a result of the decrease in the supply of vesicles from TGN, the amount of vesicles in the IS markedly decreased 1 h later (d, arrow). Note that dendrite staining is elevated in d. (e and f) β-APP::YFP was expressed overnight without (e) or with paclitaxel (f). (g and h) Kv2.1::YFP was expressed overnight without (g) or with paclitaxel (h). Kv2.1 (green) is a potassium channel sorted to the cell body and dendrites in the absence (g) and in the presence of paclitaxel (h). MAP2 was stained with red. Bars, 10 μm. (i) MT polarity is mixed in proximal dendrites after incubation with 100 nM paclitaxel overnight. (inset) Axonal MTs. Polarity of MTs is determined by the curvature of hooks in the electron micrographs (arrows). Bar, 100 nm. Electron micrograph, which shows MT organization in paclitaxel treated neurons, is available as Fig. S3. (j) Dose dependence of membrane phenotype and that of motor phenotype are similar. For membrane phenotype, percentage of neurons, which show polarized axonal transport of VSV-G::GFP are presented ($n = 3$, each 50 cells counted). For motor phenotype, percentage of neurons, which show preferential binding of rigor-KIF5 to the IS are presented ($n = 2$, each 50 cells counted). (k–n) In vitro reconstitution of preferential association of KIF5 to the MTs in the IS. Hippocampal neuronal cytoskeleton was prepared by permeabilization with 0.1% Triton X-100, and recombinant tailless-KIF5::YFP was added to the cytoskeleton (k and m). Subsequently, the cells were fixed and stained with anti-MAP2 antibody. In l and n, MAP2 staining (red) is superimposed on the KIF5 images in k and m (green). In control neurons, intense binding of KIF5 to the IS was observed (k and l, arrows), compared with other neurites. In contrast, when neurons were pretreated with 10 nM paclitaxel before permeabilization, binding of KIF5 to the axonal IS was similar to other neurites (m and n, arrows).

post-Golgi carriers, as well as tailless KIF5, be missorted to the tips of dendrites. We found that 1–10 nM paclitaxel, which inhibits MT dynamics (Derry et al., 1995) but does not inhibit the motor protein activity in vitro, drives both axonal vesicles and KIF5 to dendrites. In the presence of 10 nM paclitaxel, (1) tailless KIF5 was accumulated at dendrite tips (Fig. 5 a); (2) rigor-KIF5 failed to identify ISs (Fig. 5 b); and (3) axonal membrane proteins such as VSV-G::GFP and β-APP were missorted to dendrite tips (Fig. 5, c–f), whereas the dendrite membrane protein Kv2.1 was properly sorted (Fig. 5, g and h; Lim et al., 2000). We could examine a 1-h effect of paclitaxel treatment using VSV-G probe, which shows excellent temporal resolution, whereas normal membrane markers are gradually transported during overnight expression. Quantitative analysis revealed that the dose dependence of motor phenotype and that of membrane phenotype are quite similar (Fig. 5 j). We observed that MT organization was not significantly altered by paclitaxel at more than this dose at electron microscopic level (Fig. S4, available at http://www.jcb.org/cgi/content/full/jcb.200302175/DC1). MT polarity was mixed in proximal dendrites as reported previously (Baas et al., 1988), which was still maintained after overnight paclitaxel treatment even at 100 nM (Fig. 5 i). Time-lapse analysis revealed that the transport of tubulovesicular organelles was not inhibited at this dose of paclitaxel once the organelles entered into the axons, whereas the amount of polarized vesicles released from the TGN to the axon gradually decreased (Fig. 5, c and d; number of tubulovesicular organelles moved into axons from the TGN was 7.3 ± 1.4/100 s before paclitaxel treatment, and 0.5 ± 0.8/100 s 60 min after 10 nM paclitaxel treatment in the same neurons). As a result of the decrease of polarized transport to the IS and the extensive axonal transport from the IS, the level of transient accumulation of the VSV-G carriers in the IS decreased after 1 h incubation with 10 nM paclitaxel (Fig. 5, c and d).

To further test whether axonal targeting of KIF5 is due to the motor protein–MT-cytoskeleton interaction, or due to some indirect diffusible signals, we performed reconstitution study using Triton-permeabilized neuronal cytoskeleton and His-tag purified recombinant tailless KIF5::YFP. We found that tailless KIF5::YFP was preferentially recruited to the IS compared with dendrites and cell body (Fig. 5, k and l; fluorescence ratios of tailless KIF5::YFP in axon to dendrites was

2.2 ± 0.8 in control [n = 21], and 1.0 ± 0.3 in the presence of paclitaxel [n = 20]). In contrast, pretreatment of neurons with 10 nM paclitaxel inhibited the preferential axonal recruitment of KIF5 (Fig. 5, m and n).

MTs in the IS have distinct property from those in dendrites

Our paclitaxel experiments prompted us to see the MT dynamics around the cell body. For this purpose, we used EB1::YFP, which is known to bind to the growing tips of MTs (Tirnauer and Bierer, 2000). Although electron microscopists have long used the difference of MT organization in order to identify the IS around the cell body, their chemical property is not elucidated yet. Localization of conventional MAPs cannot explain this because, for example, although MAP2 and tau have been used as markers for dendrites and axons, MAP2 localizes in dendrites as well as in the IS, and the phosphorylated form of tau only localizes in the axons considerably distal to the IS. When we expressed EB1::YFP, in cultured hippocampal neurons, we found intense accumulation of EB1::YFP to the IS compared with the cell body and dendrites by CLSM at high Z-resolution (Fig. 6 a; see Fig. S5 a for wider field of view, available at http://www.jcb.org/cgi/content/full/jcb.200302175/DC1; fluorescence ratio of axon to dendrites was 172 ± 31.6% [n = 20]). However, CLSM cannot visualize individual growing tips of MTs in the cell body. By using CAFM, we could visualize the growing tips of MTs as EB1 dots around the cell body. In a low level of EB1::YFP expression, we could observe the movement of individual EB1 dots in both axon ISs and dendrites (Fig. 6 b; Video 8, available at http://www.jcb.org/cgi/content/full/jcb.200302175/DC1). Number of EB1 dots per 10 μm^2 per 1 min by CAFM was 4.87 ± 2.23 in the ISs, 2.16 ± 1.59 in the dendrites, and 0.77 ± 0.13 in the cell body (n = 19), which was markedly reduced to 0.58 ± 0.08, 0.20 ± 0.18, 0.13 ± 0.06, respectively after a 10-min treatment of 10 nM paclitaxel. The inhibition of MTs dynamics by the paclitaxel also decreased the speed of EB1 dots from 4.6 ± 0.9 μm/min to 1.8 ± 1.1 μm/min. We noticed that, in a higher level of EB1::YFP expression, MTs in the IS were fully decorated by EB1::YFP, whereas at the same time EB1::YFP labels only the tips of MTs as dots in the cell body and dendrites of the same neuron (Fig. 6 c, arrow; Video 9, available at http://www.jcb.org/cgi/content/full/jcb.200302175/DC1), which makes EB1::YFP an excellent marker for the axon around the cell body (Fig. 6, a and c). Control CAFM image of tubulin staining showed bright dendrite staining (Fig. 6 d). Fig. S5 shows gallery of EB1 staining (Fig. S5 b) and immuno-electron microscopy of EB1::YFP in dendrites (Fig. S5 c) and axons (Fig. S5 d). Such spatial difference of EB1 behavior within a cell was never observed in nonneuronal cells at any level of EB1 expression. Our results demonstrate unique properties of MTs in the IS compared with those in the cell body and dendrites.

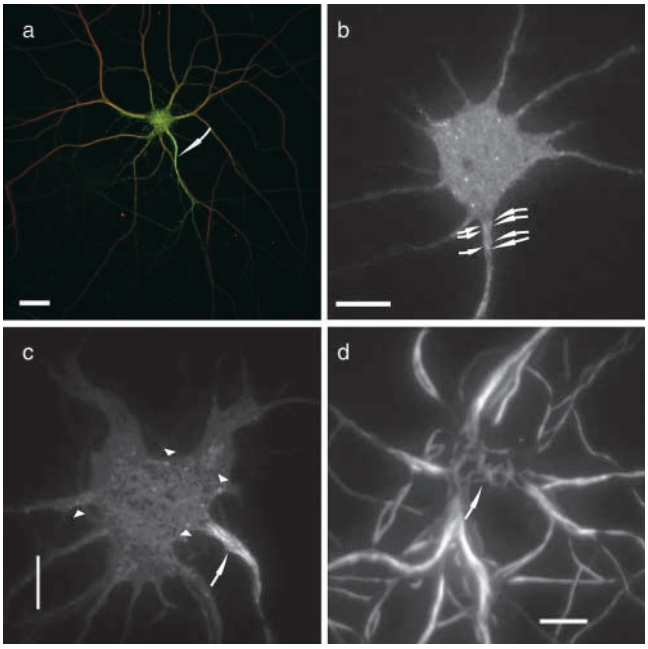

Figure 6. **MT dynamics in the IS.** (a) Maximal Z-projection of small pinhole size CLSM images of neuron transfected with EB1::YFP (green) was stained with anti-MAP2 antibody (red). EB1 extensively labeled the IS (arrow). (b and c) CAFM images of EB1::YFP expressing neurons. (b) Individual EB1 dots, which decorate the growing tips of MTs are clearly observed in dendrites, cell body, and axon in a low level of EB1::YFP expression. Note that individual EB1 dots are resolved in the IS (b, arrows; Video 8). (c) In a higher level of expression, EB1::YFP extensively labeled the MTs in the IS (c, arrow), whereas it labeled only tips of MTs in the cell body and dendrites (c, arrowheads; Video 9). (d) CAFM image of MTs stained with antitubulin antibody. Note that MTs in dendrites as well as cell bodies are visualized by CAFM. Arrow indicates MTs in the cell body. Bars, 10 μm.

Discussion

We showed that axonal tubulovesicular organelles have kinesin-driven highly processive motility in the cell body and the majority of them moved directly to the axon (Figs. 1 and 2), consistent with the idea that there is a directional cue for polarized axonal transport. We demonstrated that KIF5 motor domain, as default, has preference to the MTs in the IS (Figs. 3 and 4). Low dose paclitaxel treatment specifically blocked the polarized axonal transport of both tailless motor and tubulovesicular organelles (Fig. 5). EB1 binding revealed there is a difference in the property of MTs between dendrites and axons just around the cell body (Fig. 6). Our results collectively suggest that the MT system provides a directional cue for the preferential axonal transport of KIF5 and tubulovesicular organelles.

Polarized transport of post-Golgi axonal carriers from the trans-Golgi network to the axons

Polarized distribution of membrane proteins may be achieved by the combination of a number of different mechanisms, which include: (1) sorting of membrane proteins to different post-Golgi carriers at TGN; (2) polarized transport of the carriers to different area of the cells; (3) selective fusion between the carriers and the plasma membranes; (4) endocytosis of missorted proteins and transcytosis; (5) selective stabilization or differential turnover of certain proteins in specific regions (Hirokawa et al., 1996); and (6) diffusion barrier at the plasma membrane (Winckler et al., 1999).

In this paper, we focused on the post-Golgi transport step in neurons because sorting at the transport step may play more important role in neurons than in epithelial cells, considering the characteristic structure of neurons. As for the axonal sorting in the transport step, three statuses should be discriminated: (1) carriers are randomly transported (no sorting); (2) carriers are preferentially transported to axons in a biased manner; and (3) carriers are exclusively inhibited to enter dendrites. We found that VSV-G::GFP carriers are preferentially transported to the IS in a biased manner (Figs. 1 and 2). Its incompleteness may be covered by the sorting mechanisms in subsequent fusion or endocytosis step (Jareb and Banker, 1998). Nevertheless, the rough sorting at the post-Golgi transport step is crucial when a large volume of axonal carriers is to be transported into narrow entry of axons at the cell body. Indeed, its specific inhibition by low dose paclitaxel caused a marked accumulation of axonal carriers at dendrite tips (Fig. 5).

As for dendrite sorting in the transport step, selective inhibition of transferrin receptor carriers to enter axons was shown (Burack et al., 2000). In the case of Kv2.1, small amount of carriers appear to enter the IS. However, its amount is far smaller than VSV-G::GFP (Fig. 2 f). As a result, total distribution of Kv2.1 was somatodendritic. Low processive movement of the Kv carriers may contribute to its distribution because the carriers cannot efficiently move long distance.

Motor activity, axonal MTs, and their dynamics

Accumulation of rigor-KIF5 to the IS is interesting (Fig. 4) because it may explain the biased axonal transport of KIF5 driven tubulovesicular organelles. Tailless KIF5 also accumulated to the IS cytoskeleton in reconstitution study (Fig. 5), and tailless KIF5 was sorted to axons in transfected cells (Fig. 3). High density of MTs in the IS would contribute to this accumulation. However, the ratio of rigor-KIF5 to MTs was higher in the IS than that in dendrites. Indeed, it is possible to identify the IS by rigor-KIF5 among the dendrites, whereas simple tubulin staining cannot be a marker for axon identification. In contrast, other rigor-motor heads showed different distribution around the cell body. These results suggests a possibility that different kinesin motor heads may recognize different property of MTs between the IS and dendrites.

We found different behavior of EB1 between IS and dendrites (Fig. 6), as an independent evidence for the difference in MTs between IS and dendrites. Unexpectedly, CAFM revealed vigorous MT polymerization in the IS, whose MTs were previously thought to be stable. However, the difference in MTs became clearer when EB1 was overexpressed. EB1 fully decorates MTs in the IS, whereas it binds only growing tips of MTs in cell bodies and dendrites. These EB1 decorated MTs often extended into the cell body from the IS (Fig. S5, b7 and b8). In general, EB1 binding was thought to not reflect a chemical difference in the tubulin, but rather affinity for growing, dynamic MTs. However, the EB1 behavior in overexpressed axons appears to indicate the slowed dissociation of EB1 from the polymerized MTs, which suggests some difference in MTs between the IS and dendrites, although the mechanisms for full decoration as well as the tip decoration by EB1 are still not understood.

At present, we do not know what differences in MTs kinesin motor heads or EB1 recognized. They may recognize some posttranslational modification or some novel MAPs. A recent study revealed overlapping binding sites of yeast EB1 homologue and kinesin motors on MTs (Downing, 2000), suggesting that KIF5 also recognizes the same property of MTs in the IS. One clue is that low dose paclitaxel abolishes motor as well as vesicle sorting to axons. We do not think activity of MT dynamics directly determines the motor binding because it took an hour to inhibit the vesicle sorting, whereas 10 min was enough to inhibit MT dynamics by the addition of paclitaxel. It is well known that MT dynamics influence on the state of posttranslational modification of MTs or the binding state of new MAPs such as EB1, CLIPs, etc. (De Zeeuw et al., 1997; Tirnauer and Bierer, 2000). Thus, blockade of MT dynamics might change some MT property in the IS, which, in turn, affects KIF5 binding. Continuous MT dynamics might be necessary to maintain the difference of MTs between the IS and dendrites.

Directional cues for polarized axonal transport

Two possibilities are considered for directional cues for polarized axonal transport. One is a cytosolic diffusible signal; the other is the signal within the structural components. We observed that post-Golgi axonal carriers directly move from the TGN to the axon (Figs. 1 and 2). Our observation supports the latter possibility because the diffusible signals must always keep steep spatial difference within the cell body against their diffusion to accomplish the observed polarized axonal sorting. If diffusible signals were involved, we would observe that many axonal carriers move into the dendrites in the same side of the IS, whereas they scarcely move into the dendrites in the opposite side. This was not the case. Thus, the directional cues for the polarized axonal transport in mature neurons should be provided by structural components.

As for the directional cues in the structural components, MTs and their associated proteins would play a main role because these carriers are transported on MTs by KIF5. One possible cue is MT organization itself. Difference in MT polarity has been used to explain the polarized axonal transport (Burack et al., 2000). However, in this hypothesis, axonal carriers should be initially transported from TGN to both axon and dendrites because polarity of MTs in dendrites are mixed. Thus, MT polarity cannot explain our present observation of VSV-G carriers, and here, we would like to refer to the possible interaction of MTs with the TGN at ultrastructural level. If axonal MTs are always associated with the Golgi complex/TGN exit sites, the budded axonal carrier may naturally transported to axons. MT dynamics may be necessary to capture the new Golgi complex exit sites. Tightly packed MTs in the IS may also contribute to the axonal transport because several MTs around a single carrier could interact with multiple motors on the axonal carrier to obtain high driving power for processive movements.

The other possible cue is the regulation of MT–motor head interaction. Indeed, we found preferential KIF5 binding to the MTs in the IS, which will contribute to the polarized axonal transport. Our data collectively suggest that this MT–KIF5 interaction may play an important role in the polarized axonal sorting. Although several studies suggest that

posttranslational modification of tubulin (Liao and Gundersen, 1998; Palazzo et al., 2003) affects MT–motor interaction, little attention was paid on the regulatory role of MT–motor interaction. Although MT–motor interaction might play a role in the pathway finding for the observed TGN to the axon transport, motor tail–cargo interactions might play a role in dendrite transport (Setou et al., 2002). How motor tail–cargo interaction regulates dendritic transport is an open question for future research.

Polarity of neuron has been extensively studied from two different aspects: one is structural components (cytoskeletal organization), and the other is the transport on the cytoskeleton (membrane trafficking). Our paper suggests close relationship between MT dynamics and polarized axonal transport. Given that MT cytoskeletons are organized as a result of its dynamics, polarized membrane sorting and polarized cytoskeletal organization) may obtain the polarity information from the same source, which will be important for these apparently two different phenomena to coordinately accomplish the polarity of neurons.

Materials and methods

Cell culture and transfection

Hippocampal cells were dissociated from the E16 mouse embryo and cultured after the method of Banker and Cowan (1977) with slight modification. Cells >10 culture days were used. Adenovirus infection was performed as described previously (Nakata et al., 1998) and a modified Ca-phosphate method was used for cDNA transfection (Kohrmann et al., 1999). Results are the same when the same constructs are introduced into hippocampal neurons by either method. Recombinant adenoviruses and mammalian expression vectors in the present paper is as follows: Ad(VSV-tsO45::GFP), Ad(VSV-tsO45::YFP), Ad(VSV-tsO45::CFP::CFP), Ad(GAP-43::YFP), Ad(mouse β-APP::YFP), Ad(Kv2.1::YFP), Ad(Vamp2::CFP), Ad(EB1::YFP), Ad(kif5b T92N [1–761aa]::YFP), Ad(kif5), Ad(kif5c S205A, H206A), Ad(kif5, T93N), Ad(kif17 [1–337aa]::kif5b[327–963aa]), pEYFP-N1(kif5b[1–761aa]::YFP), pEYFP-N1(kif17[1–511aa]::YFP), pEYFP-N1(kif5b G234A[1–761aa]::YFP), pEYFP-N1(kif17 G243A [1–511aa::YFP]), pEYFP-N1(kif5b[1–327aa]::kif17[339–511aa]::YFP), pEYFP-N1(kif17 [1–337aa]::kif5b[327–761aa]::YFP), pEYFP-N1(NR2B::YFP). For immunocytochemistry, cells were washed once with prewarmed PBS and fixed with ice-cold methanol for 5 min. For permeabilization, cells were incubated with the 50 mM Pipes, 50 mM Hepes, 1 mM EGTA, and 1 mM $MgCl_2$ buffer containing 10 μM paclitaxel and 0.1% saponin at 37°C for 10 min before methanol fixation. The cells were then stained with anti-MAP2 antibody (HM2; Sigma-Aldrich), anti-GAP43 antibody (Sigma-Aldrich), or anti-β-tubulin antibody (DM1A), followed by Alexa 568-labeled secondary antibody. To avoid the effect of the thickness of the samples, data were collected by Z-sectioning at 0.72-μm intervals using the 60× oil-immersion objective (Olympus), at a small pin hole size (Iris = 2.0) of MRC1024. Data were reconstructed with maximal Z-projection. MT polarity orientation was determined using the hook method for cultured hippocampal neurons (Baas et al., 1988).

Live-cell CLSM imaging

For time-lapse double label laser scan microscopy, cells were observed using Axiovert 100 with the 40× objective (model C-APO; Carl Zeiss MicroImaging, Inc.) equipped with a confocal laser scan unit (model MRC-1024UV; Bio-Rad Laboratories). Data were collected with the confocal aperture fully open as described previously (Nakata et al., 1998). For double labeling, YFP was excited by a 488-nm Kr–Ar laser (Bio-Rad Laboratories), and CFP was excited by a 442-nm He–Cd laser (Kimmon Denki) using a fast-shutter system and time course software (Bio-Rad Laboratories). Time lag between CFP and YFP frames is ∼0.75 s

CAFM

CAFM is accomplished by using standard TIR equipment at an interface between epiillumination and TIR illumination. We used an objective-type TIR fluorescence microscope based on an inverted microscope (IX-70; Olympus) equipped with an oil-immersion objective (PlanApo 60×, NA1.4; Olympus). Specimens were illuminated with a 514-nm Ar laser or 442-nm He–Cd laser. Images of the specimen were intensified by a Gen-IV image intensifier (model C2741-21; Hamamatsu Photonics) and acquired by a chilled charge-coupled device (CCD) camera (CoolSNAP fx; Roper Scientific). Strict TIR virtually illuminates <200 nm from the surface of the coverslip. However, by carefully adjusting the incident angle of the excitation laser beam just around the critical angle, we could illuminate further deeper in the cytoplasm presumably due to the direct beam running almost parallel to the coverslip, or due to the transition phenomenon between epiillumination and TIR. For observation of post-Golgi carriers of dendrite vesicles, Kv2.1::YFP was initially expressed in the presence of brefeldin A, and was observed with CAFM microscope after extensive wash of brefeldin A.

Immuno-electron microscopy

Hippocampal cells expressing EB1::YFP or rigor-KIF5 were permeabilized with 0.1% Triton X-100, 50 mM Pipes, 50 mM Hepes, 1 mM EGTA, 1 mM $MgCl_2$, 10 μM paclitaxel at 37°C for 10 min, and were fixed with 2% PFA in the above buffer. Cells were incubated with primary antibodies followed by overnight incubation with 5-nm colloidal gold conjugated anti–mouse IgG (Amersham Biosciences). After extensive wash, cells were fixed with 2% glutaraldehyde in 0.1 M phosphate buffer. After silver enhancement (Nanoprobe, Inc.), cells were fixed after with 0.5% OsO_4, dehydrated, and embedded in Epon 812.

In vitro reconstitution

Tailless KIF5C fused with YFP tags in its COOH terminus was bacterially expressed at 18°C using pet21a vector, and His-tag purified. The hippocampal neurons were permeabilized with 10 μM paclitaxel in reconstitution buffer (0.1% Triton X-100, 100 mM Pipes, pH 6.9, 1 mM EGTA, 1 mM $MgCl_2$, 1 mg/ml BSA) at 37°C for 10 min, then incubated with 0.05 mg/ml tailless KIF5C::YFP and 3 mg/ml purified tubulin in the reconstitution buffer without paclitaxel at room temperature for 20 min, fixed with ice-cold methanol, and stained with anti-MAP2 antibody.

Online supplemental material

Fig. S1 shows double labeling of tailless-motor proteins with axon and dendrite markers. Fig. S2 shows in vitro motility assay of KIF5/KIF17 chimera motor proteins. Fig. S3 shows that KIF5 G234A and KIF17 G243A mutants strongly bind to MTs. Fig. S4 shows MT organization of 100 nM paclitaxel-treated neurons at EM level. Fig. S5 shows EB1 accumulation in the IS by CLSM, CAFM, EM. Videos 1 and 2 show CLSM image of VSV-G::GFP transport. Videos 3–5 show CAFM image of VSV-G::GFP transport (Video 3) and Kv2.1::YFP (Videos 4 and 5). Videos 6 and 7 shows CLSM image of VSV-G::GFP in neurons which overexpress full length KIF5 (Video 6) and KIF17 head and KIF5 rod and tail chimeric protein (Video 7). Videos 8 and 9 shows CAFM image of the dynamics of EB1::YFP at low expression level (Video 8) and higher expression level (Video 9). Further comments on the data reported can be found in the online legends. Online supplemental material (Figs. S1–S5, Videos 1–9, and their legends) is available at http://www.jcb.org/cgi/content/full/jcb.200302175/DC1).

We thank members of the Hirokawa lab for useful discussions.

This work was supported by a Center of Excellence grant (13CE2004) from the Ministry of Education, Sports, Science, Culture and Technology to N. Hirokawa.

Submitted: 28 February 2003
Accepted: 23 July 2003

References

Ahmari, S.E., J. Buchanan, and S.J. Smith. 2000. Assembly of presynaptic active zones from cytoplasmic transport packets. *Nat. Neurosci.* 3:445–451.

Baas, P.W., J.S. Deitch, M.M. Black, and G.A. Banker. 1988. Polarity orientation of MTs in hippocampal neurons: uniformity in the axon and nonuniformity in the dendrite. *Proc. Natl. Acad. Sci. USA.* 85:8335–8339.

Banker, G.A., and W.M. Cowan. 1977. Rat hippocampal neurons in dispersed cell culture. *Brain Res.* 126:397–442.

Burack, M.A., M.A. Silverman, and G. Banker. 2000. The role of selective transport in neuronal protein sorting. *Neuron.* 26:465–472.

Coy, D.L., W.O. Hancock, M. Wagenbach, and J. Howard. 1999. Kinesin's tail domain is an inhibitory regulator of the motor domain. *Nat. Cell Biol.* 1:288–292.

Derry, W.B., L. Wilson, and M.A. Jordan. 1995. Substoichiometric binding of taxol suppresses MT dynamics. *Biochemistry.* 34:2203–2211.

De Zeeuw, C.I., C.C. Hoogenraad, E. Goedknegt, E. Hertzberg, A. Neubauer, F. Grosveld, and N. Galjart. 1997. CLIP-115, a novel brain-specific cytoplasmic linker protein, mediates the localization of dendritic lamellar bodies. *Neuron.* 19:1187–1199.

Dotti, C.G., and K. Simons. 1990. Polarized sorting of viral glycoproteins to the axon and dendrites of hippocampal neurons in culture. *Cell.* 62:63–72.

Downing, K.H. 2000. Structural basis for the interaction of tubulin with proteins and drugs that affect MT dynamics. *Annu. Rev. Cell Dev. Biol.* 16:89–111.

Ferreira, A., J. Niclas, R.D. Vale, G. Banker, and K.S. Kosik. 1992. Suppression of kinesin expression in cultured hippocampal neurons using antisense oligonucleotides. *J. Cell Biol.* 117:595–606.

Hackney, D.D., and M.F. Stock. 2000. Kinesin's IAK tail domain inhibits initial MT stimulated ADP release. *Nat. Cell Biol.* 2:257–260.

Hirokawa, N. 1998. Kinesin and dynein superfamily proteins and the mechanism of organelle transport. *Science.* 279:519–526.

Hirokawa, N., T. Funakoshi, R. Sato, and Y. Kanai. 1996. Selective stabilization of tau in axons and MAP2c in cell bodies and dendrtites contributes to polarized localization of cytoskeletal proteins in mature neurons. *J. Cell Biol.* 132: 667–679.

Hirschberg, K., C.M. Miller, J. Ellenberg, J.F. Presley, E.D. Siggia, R.D. Phair, and J. Lippincott-Schwartz. 1998. Kinetic analysis of secretory protein traffic and characterization of golgi to plasma membrane transport intermediates in living cells. *J. Cell Biol.* 143:1485–1503.

Jareb, M., and G. Banker. 1998. The polarized sorting of membrane proteins expressed in cultured hippocampal neurons using viral vectors. *Neuron.* 20: 855–867.

Kaether, C., P. Skehel, and C.G. Dotti. 2000. Axonal membrane proteins are transported in distinct carriers: a two-color video microscopy study in cultured hippocampal neurons. *Mol. Biol. Cell.* 11:1213–1224.

Kamal, A., G.B. Stokin, Z. Yang, C.H. Xia, and L.S. Goldstein. 2000. Axonal transport of amyloid precursor protein is mediated by direct binding to the kinesin light chain subunit of kinesin-I. *Neuron.* 28:449–459.

Kanai, Y., Y. Okada, Y. Tanaka, A. Harada, S. Terada, and N. Hirokawa. 2000. KIF5C, a novel neuronal kinesin enriched in motor neurons. *J. Neurosci.* 20: 6374–6384.

Keller, P., D. Toomre, E. Diaz, J. White, and K. Simons. 2001. Multicolour imaging of post-Golgi sorting and trafficking in live cells. *Nat. Cell Biol.* 3:140–149.

Kohrmann, M., W. Haubensak, I. Hemraj, C. Kaether, V.J. Lessmann, and M.A. Kiebler. 1999. Fast, convenient, and effective method to transiently transfect primary hippocampal neurons. *J. Neurosci. Res.* 58:831–835.

Kreitzer, G., A. Marmorstein, P. Okamoto, R. Vallee, and E. Rodriguez-Boulan. 2000. Kinesin and dynamin are required for post-Golgi transport of a plasma-membrane protein. *Nat. Cell Biol.* 2:125–127.

Liao, G., and G.G. Gundersen. 1998. Kinesin is a candidate for cross-bridging MTs and intermediate filaments. Selective binding of kinesin to detyrosinated tubulin and vimentin. *J. Biol. Chem.* 273:9797–9803.

Lim, S.T., D.E. Antonucci, R.H. Scannevin, and J.S. Trimmer. 2000. A novel targeting signal for proximal clustering of the Kv2.1 K^+ channel in hippocampal neurons. *Neuron.* 25:385–397.

Miki, H., M. Setou, K. Kaneshiro, and N. Hirokawa. 2001. All kinesin superfamily protein, KIF, genes in mouse and human. *Proc. Natl. Acad. Sci. USA.* 98: 7004–7011.

Nakata, T., and N. Hirokawa. 1995. Point mutation of adenosine triphosphate-binding motif generated rigor kinesin that selectively blocks anterograde lysosome membrane transport. *J. Cell Biol.* 131:1039–1053.

Nakata, T., S. Terada, and N. Hirokawa. 1998. Visualization of the dynamics of synaptic vesicle and plasma membrane proteins in living axons. *J. Cell Biol.* 140:659–674.

Palazzo, A., B. Ackerman, and G.G. Gundersen. 2003. Tubulin acetylation and cell motility. *Nature.* 421:230.

Rice, S., A.W. Lin, D. Safer, C.L. Hart, N. Naber, B.O. Carragher, S.M. Cain, E. Pechatnikova, E.M. Wilson-Kubalek, M. Whittaker, et al. 1999. A structural change in the kinesin motor protein that drives motility. *Nature.* 402: 778–784.

Seiler, S., J. Kirchner, C. Horn, A. Kallipolitou, G. Woehlke, and M. Schliwa. 2000. Cargo binding and regulatory sites in the tail of fungal conventional kinesin. *Nat. Cell Biol.* 2:333–338.

Setou, M., T. Nakagawa, D.H. Seog, and N. Hirokawa. 2000. Kinesin superfamily protein KIF17 and mLin-10 in NMDA receptor-containing vesicle transport. *Science.* 288:1796–1802.

Setou, M., D.H. Seog, Y. Tanaka, Y. Kanai, Y. Takei, M. Kawagishi, and N. Hirokawa. 2002. Glutamate-receptor-interacting protein GRIP1 directly steers kinesin to dendrites. *Nature.* 417:83–87.

Toomre, D., P. Keller, J. White, J.C. Olivo, and K. Simons. 1999. Dual-color visualization of trans-Golgi network to plasma membrane traffic along MTs in living cells. *J. Cell Sci.* 112:21–33.

Tirnauer, J.S., and B.E. Bierer. 2000. EB1 proteins regulate MT dynamics, cell polarity, and chromosome stability. *J. Cell Biol.* 149:761–766.

Vale, R.D., T. Funatsu, D.W. Pierce, L. Romberg, Y. Harada, and T. Yanagida. 1996. Direct observation of single kinesin molecules moving along MTs. *Nature.* 380:451–453.

Winckler, B., P. Forscher, and I. Mellman. 1999. A diffusion barrier maintains distribution of membrane proteins in polarized neurons. *Nature.* 397:698–701.

Zakharenko, S., and S. Popov. 1998. Dynamics of axonal MTs regulate the topology of new membrane insertion into the growing neurites. *J. Cell Biol.* 143: 1077–1086.